ELSEVIER

Journal of Electroanalytical Chemistry 446 (1998) 67–77

JOURNAL OF ELECTROANALYTICAL CHEMISTRY

The driving force for $(p \times \sqrt{3}) \leftrightarrow (1 \times 1)$ phase transition of Au(111) in the presence of organic adsorption: a combined chronocoulometric and surface X-ray scattering study

S. Wu [a], J. Lipkowski [a,*], O.M. Magnussen [b], B.M. Ocko [b], Th. Wandlowski [c]

[a] *Department of Chemistry, University of Guelph, Guelph, Ontario N1G 2W1, Canada*
[b] *Department of Physics, Brookhaven National Laboratory, Upton, NY 11973, USA*
[c] *Department of Electrochemistry, University of Ulm, D-89069 Ulm, Germany*

Received 19 July 1997

Abstract

In situ X-ray scattering and chronocoulometric experiments were performed to assess the influence of adsorption of pyridine, 2,2′-bipyridine and uracil on the driving force for the $(p \times \sqrt{3}) \rightarrow (1 \times 1)$ transition of the Au(111) surface. We have shown that the overall driving force is a combination of the driving force due to charge and the driving force due to the adsorbate. We have estimated the magnitude of the two driving forces and have given the upper and lower limits to this estimate. Our results show that the two driving forces are of comparable magnitude and that the interpretation of the surface reconstruction phenomena given in terms of either purely charge or a purely adsorbate effect is an oversimplification.

Keywords: Gold; Organic adsorption; Crystallographic structure

1. Introduction

Under UHV conditions, clean, low-index single crystal surfaces of gold are reconstructed, i.e. the surface symmetry is different from that which would be created by simple truncation of the bulk [1–6]. It is now also well-established by various structure-sensitive techniques that, in contact with an electrolyte solution, gold electrode surfaces are reconstructed if they are negatively charged, and the reconstruction is lifted when the metal is charged positively [7–18]. This behavior is consistent with electronic theories which explain reconstruction of Au surfaces in vacuum in terms of a compressive stress of s-p electrons balanced by a repulsive interaction of the filled d-shells [19–23]. Negative charging of the metal surface increases the density of s-p electrons and hence increases the compressive stress. The stress forces surface atoms to form a more tightly packed reconstructed structure. In contrast, positive charging of the surface decreases the density of s-p electrons and hence reduces the compressive stress. The surface atoms relax therefore into the more open (1×1) structure.

Although this explanation is attractive, one has to be cautious in applying a theory developed for the metal|vacuum interface to describe phenomena at the metal|solution interface. In situ STM and SXS measurements have shown that the potential induced structural transition due to reconstruction or its lifting changes the density of surface gold atoms [7,24,25]. The excess of gold atoms is expelled during the $(p \times \sqrt{3}) \rightarrow (1 \times 1)$ transition of the Au(111) surface and the diffusing atoms coalesce to form islands of monoatomic height [7–17]. Anions adsorb preferentially on steps, and their chemisorption weakens the gold-gold bond, and hence

* Corresponding author. Fax: +1 519 7661499; e-mail: lipkowski@chembio.uoguelph.ca

0022-0728/98/$19.00
PII S0022-0728(97)00607-4

they facilitate the lifting of the reconstruction[7]. Organic molecules may reduce [26,27] or increase [25,28–30] the stability range of the reconstructed surface. These observations were discussed recently by Kolb [7]. Often the amount of adsorbed anions or adsorbed molecules changes in a quasi-linear fashion with the charge on the metal [7,25,26,28]. For this reason, it is difficult to establish whether the reconstruction is lifted by the change of surface charge or as a result of the ionic or molecular adsorption [7,25,28].

In general the driving force for the change of the surface reconstruction is a difference of the surface energy of a solid electrode between the reconstructed $\gamma(\mathrm{R})$ and unreconstructed $\gamma(\mathrm{U})$ surface[19] (γ is called a superficial work according to the notation used recently by Lang and Heusler [31]). In the absence of adsorbates ($\theta = 0$) the driving force is equal to:

$$\Delta\gamma_{\theta=0} = \gamma_{\theta=0}(\mathrm{R}) - \gamma_{\theta=0}(\mathrm{U}) \quad (1)$$

and in the presence of adsorbates it is given by:

$$\Delta\gamma_{\theta} = \gamma_{\theta}(\mathrm{R}) - \gamma_{\theta}(\mathrm{U}) \quad (2)$$

Eqs. (1) and (2) may be combined and the change of the surface energy in the presence of adsorbates may be conveniently expressed in terms of $\Delta\gamma_{\theta=0}$ and an additional term $\Delta\phi$:

$$\Delta\gamma_{\theta} = \Delta\gamma_{\theta=0} - \Delta\phi \quad (3)$$

where $\Delta\phi = \phi(\mathrm{R}) - \phi(\mathrm{U})$ with $\phi(\mathrm{R}) = \gamma_{\theta=0}(\mathrm{R}) - \gamma_{\theta}(\mathrm{R})$ and $\phi(\mathrm{U}) = \gamma_{\theta=0}(\mathrm{U}) - \gamma_{\theta}(\mathrm{U})$. The difference between the surface energy of an electrode in the absence and in the presence of an adsorbate is called the surface pressure [32]. Therefore, $\phi(\mathrm{R})$ and $\phi(\mathrm{U})$ are the surface pressures of adsorbates at a reconstructed and an unreconstructed surface, respectively. In Eq. (3), the first term may be considered as a driving force for the charge-driven and the second term as a driving force for the adsorbate-driven change of the surface structure. If $\Delta\phi$ is positive the reconstructed surface is stabilized by adsorption. When $\Delta\phi$ is negative the adsorption assists lifting of the reconstruction. It is only when $\Delta\phi$ is equal to zero, that the surface reconstruction could be explained solely in terms of a change of the charge density at the electrode surface.

One has to measure the surface pressure for the adsorbed species at the unreconstructed and reconstructed surfaces, and to calculate their difference $\Delta\phi$, in the potential (charge) range where the structural change at the surface takes place, to estimate the driving force due to the adsorbate. The measurements have to be extended to potentials (charges) at which either the (1×1) or the reconstructed surfaces are metastable. These measurements are feasible, provided the kinetics of the surface reconstruction phenomena are slow enough for the predetermined surface crystallography to be preserved in the thermodynamically forbidden region, at least for a period of time long enough to measure the film pressure of an adsorbed ion or molecule. The processes of lifting of the surface reconstruction in the presence of specifically adsorbed anions are usually too fast to perform reliable measurements of the film pressure [24]. However, in part I of this project, we have recently shown, that the adsorption of aromatic heterocycles such as pyridine, bipyridine and uracil significantly slows down the lifting or restoration of the reconstructed Au(111) surface [29]. The reconstructed and unreconstructed structures of the surface exist in a sufficiently wide potential interval as metastable states, for a period of time ranging from seconds to several minutes. These results are also supported by recent in situ STM experiments with uracil [28] and 2,2′-bipyridine [30,33]. We will demonstrate in this work that, due to the sufficiently long lifetime of the metastable states, the charge densities at the (1×1) and $(\mathrm{p} \times \sqrt{3})$ surfaces could be measured over a broad range of electrode potentials. These charge densities can then be used to calculate the surface pressure of adsorbed organic molecules and the film pressure difference $\Delta\phi$. In this way, the impact of organic adsorption on the surface crystallography of the substrate can be assessed. We will also show that the charge density curves could be used to estimate the magnitude of the total driving force for the phase change $\Delta\gamma_{\theta}$.

In brief, the objectives of this work were to: (i) measure the charge density data for the reconstructed and unreconstructed Au(111) surface in the presence and absence of pyridine, 2,2′-bipyridine and uracil, (ii) use the charge density data to calculate the surface pressure for the adsorption of molecules at the (1×1) and $(\mathrm{p} \times \sqrt{3})$ surfaces, (iii) determine the values of $\Delta\phi$ and estimate the values of $\Delta\gamma_{\theta}$, (iv) assess the role played by the molecular adsorption and the charge on the metal in causing a change of the crystallographic structure of the substrate.

2. Experimental

The X-ray scattering measurements were carried out at Brookhaven National Laboratory. A focused monochromatic radiation ($\lambda = 1.542$ Å) at the beamline X22B of the National Synchrotron Light Source was used. The electrode was a disk-like Au(111) single crystal oriented within 0.1° of the surface normal axis. Detailed information about the setup and procedure can be found in [24] and in part I of this project [29].

The methodology of the electrochemical experiments performed to determine electrode charge density has been described elsewhere [34,35]. The electrode was a gold single crystal grown, cut, and polished in our laboratory. The flame-annealing technique was used to clean the electrode before each experiment, and the

hanging meniscus configuration was employed during the measurements. The supporting electrolyte was 0.1 M $KClO_4$ prepared from Milli-Q (18 MΩ cm) water. Pyridine (Fisher 99.95%) was used without purification, however 2,2′-bipyridine and uracil (Aldrich) were further purified by sublimation or recrystallization before use. A custom software was used to control the chronocoulometric experiments and collect data through an IBM 386 PC which was interfaced to a PARC 173 potentiostat by a RC-16 electronics board. All potentials are reported versus the saturated calomel electrode (SCE).

3. Results and discussion

3.1. Surface X-ray scattering studies

Details of the surface X-ray scattering experiments and results were described in the preceding paper [29]. Here we will present only the material which is needed for the discussion of the thermodynamic data. The Au(111) surface reconstruction is characterized by a uniaxial compression of the top layer of gold atoms. The reconstruction forms a rectangular unit cell usually termed as $(p \times \sqrt{3})$. In the SXS experiment, the $(p \times \sqrt{3})$ reconstruction gives rise to additional in-plane superstructural reflections beyond the underlying (1×1) pattern. Because of the three symmetry equivalent reconstruction domains (rotated by 120° from each other), the additional reflections are arranged in a hexagonal pattern surrounding the integer (H,K) positions. Fig. 1 shows the characteristic reciprocal space pattern of equal intensity contours in the vicinity of the (0,1) reflection [24].

The potential dependence of the surface structure was studied by measuring the scattering profiles through the (0,1) reflection and one of two surface reflections with the largest wave vector transfer at $L = 0.2$. The scan direction is labeled q_r in the inset to Fig. 1. The corresponding in plane projection of the scattering wave vector for such a scan is given by $(q_r/\sqrt{3}a^*,\ 1 + q_r/\sqrt{3}a^*)$. The experiment started either with an electrochemically reconstructed Au(111)–$(p \times \sqrt{3})$ surface at $E = -800$ mV, or with an unreconstructed Au(111)–(1×1) electrode at $E = 700$ mV. The potential step was set to 20 mV and an effective potential sweep rate was 0.25 mV s^{-1}. Fig. 1 shows two typical scattering profiles, measured at different potentials. The first peak at $q_r = 0$ corresponds to the (0,1) reflection which originates from the termination of the bulk gold crystal and is strongest when the surface is (1×1). The second peak corresponds to the superlattice reflection, here localized around (0.022,1.022). The intensity and position of this peak is directly related to the size and incommensurability of the reconstructed superlattice. Therefore, one can readily determine the degree of reconstruction from such a profile [24,29]. At negative potentials where the surface is reconstructed (-738 in Fig. 1), both reflections, e.g. at (0,1) and (0.022,1.022), show comparable intensities. Here the second peak corresponds to the position $q_r = \delta a^* = 0.022a^*\sqrt{3} = 0.038a^*$ [24]. The stripe separation $pa = a\sqrt{3}/(2\delta)$ is equal to $23a$ when $\delta = 0.038$ [24]. At positive potentials where the reconstruction is lifted (612 mV in Fig. 1), the intensity of the (0,1) peak increases significantly while the (0.022,1.022) peak is rather small Here, we will use the dependence of the intensity of the (0,1) peak to monitor the changes of the surface structure.

Fig. 2 shows the (0,1) intensity as a function of potential for the system of 0.1 M $KClO_4$ electrolyte and with the addition of pyridine (top panel), 2,2′-bipyridine (middle panel), and uracil (bottom panel). The symbols and solid lines show intensities measured in the presence of the organic molecules. The dotted line in each panel represents the changes of the (0,1) intensity in the pure $KClO_4$ solution. The arrows indicate directions of the voltage scan. The reconstructed $(p \times \sqrt{3})$ structure could be conserved in a potential

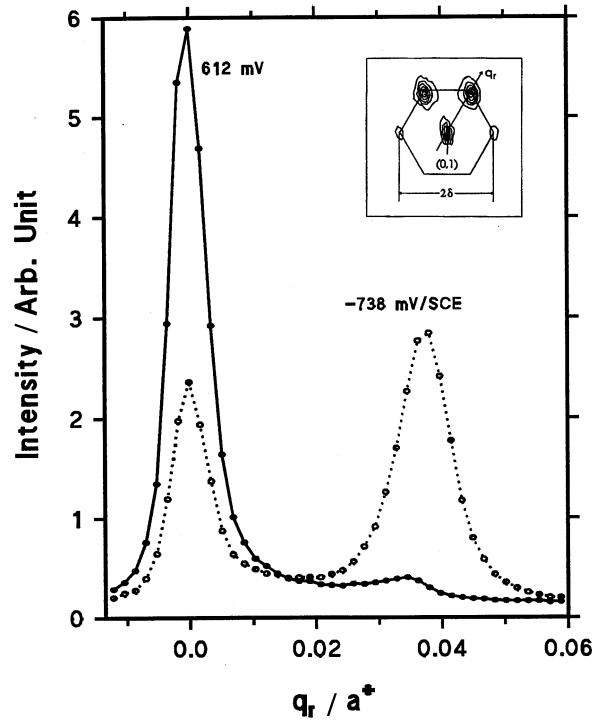

Fig. 1. X-ray scattering profiles along q_r at $L = 0.2$ for the Au(111) surface at potentials of -738 (open points and dotted line) and 612 mV (SCE) (black points and solid line) in a solution of 0.1 M $KClO_4 + 1.0 \times 10^{-2}$ M pyridine. Inset: schematic representation of the reciprocal space pattern for the Au(111) surface around the low-order bulk-reflection (0,1) at $L = 0.5$. The four satellite spots originate from the $(p \times \sqrt{3})$ reconstructed phase with its three rotationally equivalent domains. The axis q_r is defined to be along the [1,1] direction. The inset is reproduced from Ref. [24].

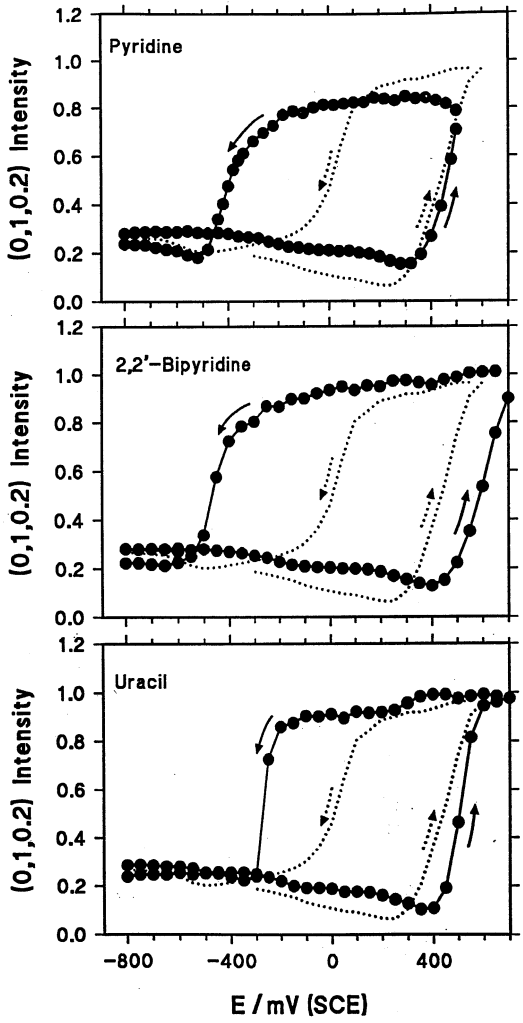

Fig. 2. Potential dependence of the integrated (0,1,0.2) intensity for the Au(111) surface in 0.1 M $KClO_4$ with with 1.0×10^{-2} M addition for each; pyridine (top panel), 2,2′-bipyridine (middle panel) and uracil (bottom panel). Dotted lines represent the intensity curve recorded in the pure 0.1 M $KClO_4$ solution. Arrows indicate the direction of the voltage scan.

range from -800 to $\sim +270$ mV, in the pure supporting electrolyte. The (0,1) intensity increased abruptly at ~ 270 mV which indicates the lifting of the reconstruction. At about 500 mV, it reaches its maximum plateau indicating the complete formation of a well established, ordered (1×1) surface. The reconstruction could then be restored after the potential was changed to a value lower than 100 mV. With the addition of pyridine to the electrolyte, the lifting of reconstruction starts at $E > 270$ mV, and is completed within the time scale of the chosen scan rate at $E > 500$ mV. Relative to the case of a pure supporting electrolyte, the restoring of the reconstruction is shifted 400 mV towards more negative potentials. The presence of 2,2′-bipyridine and uracil pushed the lifting of reconstruction to a potential more positive than 270 (to about 600 mV with 2,2′-bipyridine and 500 mV with uracil). Both molecules form highly ordered chemisorbed phases at these potentials [28,30]. In these two solutions, the reconstruction was reformed also at quite different potentials (at about -450 for 2,2′bipyridine and -250 mV for uracil). These results clearly demonstrate that the potentials at which the reconstruction was lifted and recovered were affected significantly by the addition and nature of the three organics. The reconstruction-deconstruction processes always show significant hysteresis of the potentials at which these phase transitions occur. The presence of organics in the solution hinders the reaction and increases the hysteresis. The slow kinetics of the surface reconstruction-deconstruction phenomena make the measurements of charge densities at the reconstructed and unreconstructed surfaces feasible as described below.

3.2. Potentials of zero charge of the $(p \times \sqrt{3})$ and (1×1) Au(111) surfaces

In order to discuss the energetics of the lifting and restoring of the reconstruction, we have to determine the charge density at the reconstructed and unreconstructed surfaces. The first step in this procedure is to determine the potential of zero charge for the two surfaces. The pzc of the reconstructed and unreconstructed surfaces were measured in 1.0×10^{-3} M $KClO_4$ solution. It is known that the pzc of the Au(111) electrode does not depend on the concentration of perchlorate ion [36,37] and hence the value of the pzc determined for this dilute electrolyte could be used for the 0.1 M $KClO_4$ solution as well. To determine the pzc of the $(p \times \sqrt{3})$ surface, the electrode was held at -800 mV for a period of 5 min to ensure that the surface was reconstructed. Then the potential was stepped to a more positive value, close to the pzc. A small sinusoidal perturbation (5 mV rms, 250 Hz) was applied and the differential capacity of the surface was recorded for a period of 200 ms. The SXS scattering experiments indicated that the initial state of the surface is not changed during such a short period of time. The above procedure was repeated for a series of potentials around the pzc and the differential capacity was plotted as a function of potential The pzc was found from the position of the minimum on this plot. The same procedure was employed to determine the pzc of the (1×1) surface. In this series of measurements the potential was initially held at $+600$ mV for a period of 5 min, to ensure that the reconstruction was lifted, before the potential was stepped to a value around the pzc.

The differential capacity curves for the reconstructed and unreconstructed surfaces, determined from the above experiments, are shown in Fig. 3. The solid lines are the polynomial fits to the data. The curves are quite

smooth in the potential range close to the pzc. The data become slightly scattered at potentials far beyond the potential of zero charge. The pzc determined for the electrochemically reconstructed Au(111)–(p × √3) and the Au(111)–(1 × 1) surfaces are 270 mV and 230 mV versus SCE, respectively. The values measured previously by Kolb et al. [7,38] were 320 mV for the (p × √3) surface and 230 mV for the (1 × 1) surface. Apparently, the value of the pzc for the reconstructed surface, reported in [38], is much higher than our result. These discrepancies may be explained by a different treatment of the electrode surface used in our work and in Ref. [38]. Kolb et al. measured the pzc at a freshly flame-annealed surface, where usually entire terraces are covered with one uniform domain of the chevron like structure [7]. In contrast, our experiments were made on an electrode for which the flame induced reconstruction was lifted and later was restored in situ by applying a negative electrode potential. Under these conditions, the individual terraces of the gold surface contain a large number of small, rotationally equivalent domains of the reconstructed phase. In comparison to the thermally annealed electrodes, these surfaces exhibit a significantly higher defect density (domain boundaries within the reconstructed phase). The negative shift of the pzc with increasing defect density was also reported by Leceour et al. [39] for stepped surfaces. We would like to emphasize that all SXS and charge density measurements reported here were performed on a surface where reconstruction was potential induced rather than induced by flame-annealing.

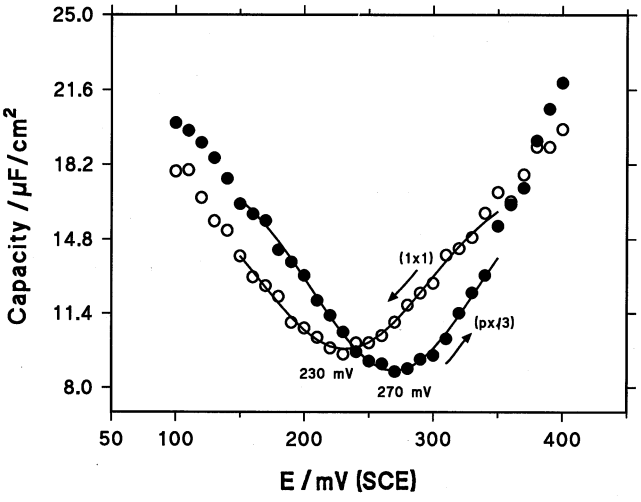

Fig. 3. Potential dependence of the differential capacity for the reconstructed (p × √3) and unreconstructed (1 × 1) Au(111) surfaces in 1.0×10^{-3} M $KClO_4$ solution. The pzc for each surface was determined from the position of the minimum of the corresponding curve.

3.3. Charge densities for the (p × √3) and (1 × 1) surfaces

In the presence of pyridine, Skoluda et al. [40] measured the charge density for the reconstructed and unreconstructed Au(100) surface in a broad range of electrode potentials. We have used similar methodology to measure charge densities for the (p × √3) and (1 × 1) surfaces of the Au(111) electrode. The charge density for the reconstructed surface was determined in the following way. The electrode potential was held at − 800 mV for 5 min to ensure that the surface was reconstructed and then stepped to a more positive value E. The charge difference ΔQ between these two potentials was recorded within a short period of time (− 150 ms). The potential E was varied sequentially from − 775 mV to + 600 mV using 25 mV increments and the values of ΔQ were determined for this whole region. The pzc value for the reconstructed surface was used to convert the charge difference into the absolute charge density according to the procedure described in [34,35].

A similar program was used to determine the charge density for the unreconstructed surface. This time the potential was initially held at a value which was positive enough to lift the reconstruction but was sufficiently negative to prevent oxide formation at the surface. A different values for this potential was chosen for each organic molecule. The SXS data and cyclic voltammograms were used to select the optimal value of the initial potential. The potential was then stepped in the negative direction and the charge difference ΔQ was measured during a period of ∼150 ms. This procedure was repeated, stepping to progressively more negative potentials until the values of ΔQ were determined for potentials extending up to the negative limit determined by the stability range of the Au(111) structure. The value of the pzc for the unreconstructed surface was used to convert the difference of the charge densities into the absolute values of Q. The shape of the charge-time curves, recorded in the potential step experiments, indicated that the adsorption-desorption kinetics were fast enough for the adsorption equilibrium between the electrode surface and the bulk of the solution to be established during the 150 ms time window [24,29].

Fig. 4 shows the absolute charge density data determined for the reconstructed and the unreconstructed surfaces in the presence of pyridine, 2,2′-bipyridine and uracil. For comparison, the charge density data for the reconstructed and unreconstructed Au(111) surfaces in the organics-free supporting electrolyte, are included in each panel. The charge versus potential curves for pyridine and uracil have quite a similar shape for the two surfaces. However, the differences between the two curves are pronounced in the case of bipyridine. The curves for the unreconstructed surface are apparently

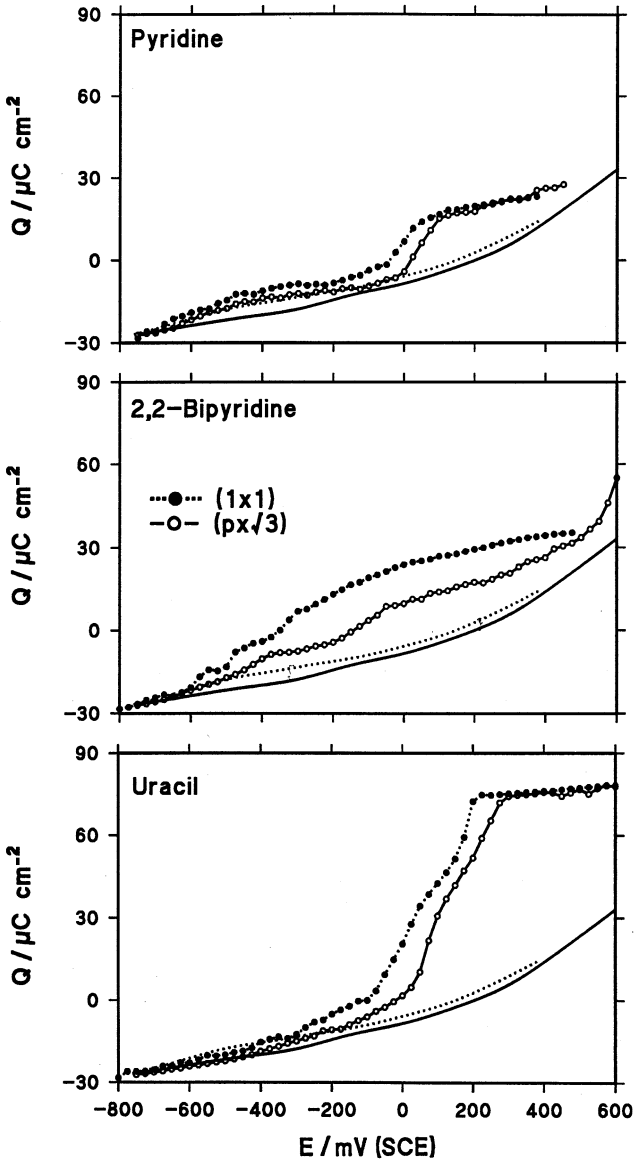

Fig. 4. Potential dependence of charge density determined for Au(111) surfaces in a solution of 0.1 M $KClO_4$ with and without 1.0×10^{-2} M of each; pyridine (top panel), 2,2′-bipyridine (middle panel) and uracil (bottom panel). In each panel, solid line and open points mark the plots determined for the reconstructed $(p \times \sqrt{3})$ surface. Dotted lines with black points mark the plots for the (1×1) surface. The solid and dotted lines without points mark the charge density plots for the reconstructed and unreconstructed surfaces in the pure 0.1 M $KClO_4$ electrolyte.

shifted slightly towards negative potentials relative to the plots representing the reconstructed surface. In the presence of organic molecules, this shift is more pronounced than in the pure supporting electrolyte.

The SXS studies reported in [24,29], and also SHG data [18], indicate that, under experimental conditions comparable to those employed in this work, the time needed to lift or restore the surface reconstruction is longer than a few seconds. The time window, within which the charge densities shown in Fig. 4 were measured, was at least an order of magnitude smaller than the time needed for the surface structural changes to occur. Therefore, the charging of the interface took place effectively at a structurally frozen surface. Consequently, these charge densities represent a state in which the surface is in equilibrium with the electrolyte solution but not in equilibrium with the bulk of the solid electrode.

3.4. Surface pressures for the $(p \times \sqrt{3})$ and (1×1) surfaces

Lang and Heusler [31] demonstrated recently (see also Parsons [41]), that the electrocapillary equation may be applied to describe an electrode surface, which is in equilibrium with the bulk of the solution but not in equilibrium with the bulk of the solid. Using this approach, the change of the surface energy (superficial work) is given by the expression:

$$-\mathrm{d}\gamma = Q\mathrm{d}E + \Gamma\mathrm{d}\mu + (\gamma - \Upsilon)\mathrm{d}\epsilon \qquad (4)$$

where Γ is the Gibbs excess of organic compound, μ is its chemical potential in the bulk of the solution, and Q is the surface charge density. This charge density is equal to the sum of two terms: $Q = \sigma_M + \sigma_e$, where σ_M is the charge corresponding to the state of equilibrium between the surface and the bulk of the solid electrode, and σ_e is the additional charge due to the presence of mechanical stress which builds up locally when the interface of the solid electrode is not in equilibrium with the solid bulk. For example, at potentials at which the reconstructed surface is stable, the segment of the charge density plot representing the $(p \times \sqrt{3})$ surface, may be considered as representing the equilibrium between the surface and the bulk of the gold electrode. The charge Q is then equal to σ_M. In contrast, in the same potential range, the segment of the charge density plot corresponding to the (1×1) surface represents a metastable state of the surface which experiences a local mechanical stress. The measured charge is then equal to $Q = \sigma_M + \sigma_e$ with the magnitude of σ_e being approximately determined by the difference between the two charge density curves taken at constant potential.

Symbols Υ and ϵ in the last term of Eq. (4) denote surface stress and surface strain, respectively. The magnitude of this term was a point of a controversy. Some of the recent direct surface stress measurements suggested that this term may be large [42–44]. The implications of these direct surface stress measurements for the thermodynamics of the solid|solution interface were discussed recently in [45]. It was shown in [45] that $\mathrm{d}\epsilon \approx 5 \times 10^{-8}\,\mathrm{d}\Upsilon$, and that the last term is negligibly small even if the potential or adsorption induced changes of the surface stress are much larger than the changes of the superficial work. Therefore, in the data analysis presented below, this term is neglected.

In order to assess the role played by adsorbate and charge on the metal in causing a change of the surface crystallography, we have to use charge as the independent electrical variable. To measure the driving force of surface reconstruction at a constant charge, it is convenient to introduce the Parsons function $\xi = \gamma + QE$ and to convert Eq. (4) to the following form [46]:

$$d\xi = E dQ - \Gamma d\mu \quad (5)$$

The surface pressure at a constant charge is than equal to $\phi = (\xi_{\theta=0} - \xi\theta)$, with $\xi_{\theta=0}$ and ξ_θ being the Parsons functions for the electrode in the absence and presence of organic adsorbates [32]. The surface pressure can be conveniently determined from the measured charge density plots, by applying the relationship:

$$\phi = \int_{Q_{\theta=0}}^{Q_\theta} (E_{\theta=0} - E_\theta)_Q dQ \quad (6)$$

where $(E_{\theta=0} - E_\theta)_Q$ represents a difference between electrode potentials for the organic free and the organic covered electrode, taken at a constant charge. In this case, Q becomes the variable and E the integrand. The integration begins at charges where the organic molecules are desorbed from the electrode surface and continues over the range of charges in which they are adsorbed at the interface.

As an example, Fig. 5 shows the surface pressures at constant charge for the reconstructed and unreconstructed surfaces of Au(111) in the presence of pyridine. The surface pressures display a small but measurable dependence on the crystallographic structure of the electrode surface. Significantly, the surface pressure plots for the (1×1) and $(p \times \sqrt{3})$ surfaces intersect each other indicating that the pyridine molecules display preferential adsorption on either (1×1) or $(p \times \sqrt{3})$ surfaces in different regions of the electrode charge density. It is convenient to discuss the differences between the energetics of molecular adsorption at the two electrode surfaces by examining how $\Delta\phi = \phi(p \times \sqrt{3}) - \phi(1 \times 1)$ changes with the electrode charge density. Fig. 6 shows plots of $\Delta\phi$ versus Q for the three organic molecules investigated. For all three molecules, the $\Delta\phi$ values cross zero at about -3 μC cm^{-2}. At smaller charge densities, the values of $\Delta\phi$ are positive and at higher charges they are negative. A positive value of $\Delta\phi$ indicates that the organic molecule displays a preferential adsorption at the reconstructed surface and a negative value indicates a preferential adsorption at the unreconstructed surface. Therefore, the present results show that the adsorption of the organic molecules is stronger at the reconstructed surface when the electrode surface is charged negatively and displays a stronger adsorption at the unreconstructed surface if it is positively charged. The change in the character of preferential adsorption is observed at small negative charges. It is useful to recall that the positive values of $\Delta\phi$ represent a driving force for the adsorbate induced reconstruction of the electrode surface and that the negative values represent the driving force for the adsorbate induced lifting of the reconstruction. The driving forces are small but not negligible. The present result shows that the changes of the electrode surface structure observed in the presence of organic molecules may be at least partially driven by the adsorbate.

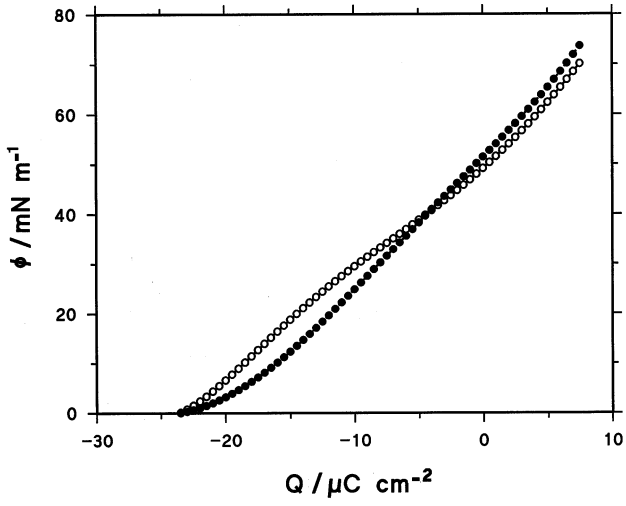

Fig. 5. Charge density dependence of the surface pressure for 0.1 M $KClO_4 + 1.0 \times 10^{-2}$ M pyridine solution at reconstructed $(p \times \sqrt{3})$ surface (open points) and unreconstructed (1×1) Au(111) surface (black points).

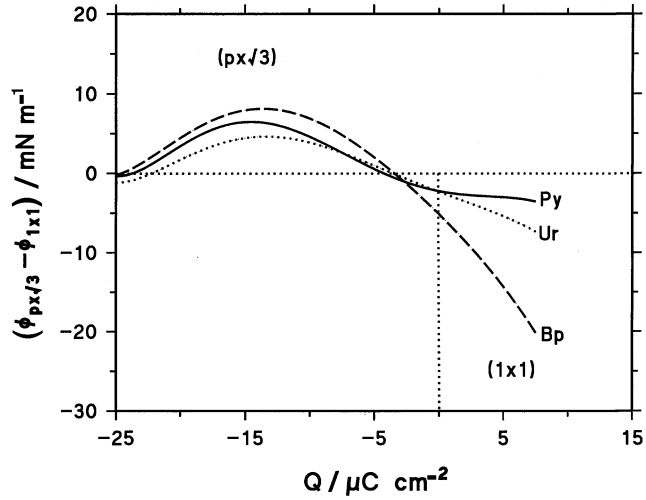

Fig. 6. Difference between the surface pressure of pyridine at constant charge at the $(p \times \sqrt{3})$ and (1×1) surfaces, $\Delta\phi$, versus the charge at the Au(111), for 0.1 M $KClO_4 + 1.0 \times 10^{-2}$ M pyridine solution.

3.5. The driving force for surface reconstruction

In this section we will estimate the overall driving force for lifting/restoring of the surface reconstruction. Eq. (3) applies only to the case when the charge Q at the reconstructed and unreconstructed surface is equal

to zero. For other charge densities, a distinction has to be made between the driving force at a constant electrode potential and at a constant charge. The portion of the surface energy due to the charge on the surface is different in the two cases. When the driving force is calculated at a constant electrode potential, symbol $\pi = \gamma_{\theta=0} - \gamma_\theta$ is used to denote the surface pressure [32] and the expression for the driving force is:

$$\Delta\gamma_\theta = \Delta\gamma_{\theta=0} - \Delta\pi \tag{7}$$

where $\Delta\pi = \pi(\mathrm{R}) - \pi(\mathrm{U})$. For each of the two states of the surface, the film pressure at a constant potential may be conveniently calculated by integration of the charge density plots in Fig. 4 treating E as the variable and Q as the integrand:

$$\pi = -\int_{E_{\theta=0}}^{E_\theta} (Q_\theta - Q_{\theta=0})_E \mathrm{d}E \tag{8}$$

Note that, depending on the choice of the independent variable, the same set of experimental data gives the surface pressures at constant charge or at constant potential. To calculate the driving force of reconstruction at a constant charge, the Parsons function should be used and the driving force is then expressed as:

$$\Delta\xi_\theta = \Delta\xi_{\theta=0} - \Delta\phi \tag{9}$$

where $\Delta\xi_\theta = \xi_\theta(\mathrm{R}) - \xi_\theta(\mathrm{U})$ and $\Delta\xi_{\theta=0} = \xi_{\theta=0}(\mathrm{R}) - \xi_{\theta=0}(\mathrm{U})$. Eq. (3) is a specific case of the more general Eq. (9).

We have already learned how to determine $\Delta\phi$ or $\Delta\pi$. Now we will attempt to estimate the terms $\Delta\gamma_{\theta=0}$ and $\Delta\xi_{\theta=0}$. It is convenient, for this purpose, to integrate Eq. (4) at a constant composition of the solution ($\mathrm{d}\mu = 0$) and to express $\Delta\gamma_{\theta=0}$ by the following function:

$$\Delta\gamma_{\theta=0} = \gamma_{Q=0}(\mathrm{R}) - \gamma_{Q=0}(\mathrm{U}) - \left(\int_{E_{Q=0}}^{E_Q} Q_{\theta=0}(\mathrm{R})\mathrm{d}E - \int_{E_{Q=0}}^{E_Q} Q_{\theta=0}(\mathrm{U})\mathrm{d}E\right) \tag{10}$$

Likewise, we may integrate Eq. (5) to get the following expression for $\Delta\xi_{\theta=0}$:

$$\Delta\xi_{\theta=0} = \gamma_{Q=0}(\mathrm{R}) - \gamma_{Q=0}(\mathrm{U}) + \left(\int_{Q=0}^{Q_E} \mathrm{E}_{\theta=0}(\mathrm{R})\mathrm{d}Q - \int_{Q=0}^{Q_E} E_{\theta=0}(\mathrm{U})\mathrm{d}Q\right) \tag{11}$$

where the integrands $Q_{\theta=0}(\mathrm{R})$ and $Q_{\theta=0}(\mathrm{U})$ are the charge plots in Fig. 4 determined for the pure $KClO_4$ solution and integrands $E_{\theta=0}(\mathrm{R})$ and $E_{\theta=0}(\mathrm{U})$ are given by the same plots when the charge is treated as a variable. The integration constants $\gamma_{Q=0}(\mathrm{R})$ and $\gamma_{Q=0}(\mathrm{U})$ are the surface energies at the potentials of zero charge of the reconstructed and unreconstructed surface, respectively. Note, that when charge is equal to zero, $\xi = \gamma$, and, therefore, the same integration constants appear in Eqs. (10) and (11). The two integrals can easily be calculated by integration of the corresponding curves in Fig. 4. The difference, $\gamma_{Q=0}(\mathrm{R}) - \gamma_{Q=0}(\mathrm{U})$, must to be determined independently. We would like to emphasize that the absolute values of the surface energies for a solid electrode cannot be measured, these quantities could only be estimated.

Ross and D'Agostino [47] and Gao et al. [48] have pointed out that the structural phase transition should occur thermodynamically at the crossing point between the electrocapillary curves for the (1×1) and $(\mathrm{p} \times \sqrt{3})$ surfaces (E_T). This is the potential at which $\Delta\gamma_\theta = 0$. If we know the potential at which $\Delta\gamma_\theta = 0$, the difference $(\gamma_{Q=0}(\mathrm{R}) - \gamma_{Q=0}(\mathrm{U}))$ and the values of $\Delta\gamma_\theta$ for all other potentials can easily be calculated. For the Au(100) electrode, Ross and D'Agostino and Gao et al. made attempts to calculate the electrocapillary curves for the reconstructed and unreconstructed surface by integration of the differential capacity data and to evaluate the potential at which they cross. Ross and D'Agostino adjusted the relative position of the electrocapillary curves taking the calculated difference between the surface energies for the reconstructed and unreconstructed surface in vacuum [19]. Gao et al. assumed that the thermodynamic potential of lifting the reconstruction corresponds to the potential at which lifting of the reconstruction was observed by STM. The two estimates differ significantly. We will show below that for the Au(111) surface, by calculating the surface energy changes from electrode charge densities and estimating the potential range within which the reconstruction should be lifted from SXS data [29], we may give a more precise estimate of the driving force and the thermodynamic potential of the phase transition than the estimates made in the past.

We will assume as a first estimation that $(\gamma_{Q=0}(\mathrm{R}) - \gamma_{Q=0}(\mathrm{U})) = 0$. The driving force for the phase transition is than equal to:

$$\Delta\gamma_\theta = -\left(\int_{E_{Q=0}}^{E_Q} Q_\theta(\mathrm{R})\mathrm{d}E - \int_{E_{Q=0}}^{E_Q} Q_\theta(\mathrm{U})\mathrm{d}E\right) - \Delta\pi \tag{12}$$

which may be calculated by integration of the charge density data. Fig. 7 shows the calculated values of $\Delta\gamma_\theta$ versus potential for the three organic molecules and the pure potassium perchlorate solution. The horizontal bars in Fig. 7 show the position and length of the potential range within which the hysteresis of the (0,1) intensity was observed in Fig. 2. For each bar, the positive limit corresponds to the potential at which the (0,1) intensity attains 50% of its maximum value and the negative limit corresponds to the potential at which the intensity drops to 50% of the maximum value. All curves in Fig. 7 cross the zero line. If our estimation is correct, the point at which a $\Delta\gamma_\theta$ curve crosses the zero line ($\Delta\gamma_\theta = 0$) corresponds to the thermodynamic poten-

tial of the phase transition E_T. For each solution, the thermodynamic potential at which the reconstruction is lifted or restored must be located within the limits determined by the hysteresis loop marked by the corresponding bar. In Fig. 7, all the crossing points are located within the corresponding hysteresis bars. Therefore, the first estimation seems to be reasonable.

We will consider now the case, where the difference $(\gamma_{Q=0}(R) - \gamma_{Q=0}(U))$ is not equal to zero. In this case, all $\Delta\gamma_\theta$ curves in Fig. 7, should be shifted up or down the $\Delta\gamma_\theta$ axis by an amount equal to $(\gamma_{Q=0}(R) - \gamma_{Q=0}(U))$. Such a shift will change the potential at which a given $\Delta\gamma_\theta$ plot crosses the zero line. This behavior imposes an upper and a lower limit onto the $(\gamma_{Q=0}(R) - \gamma_{Q=0}(U))$ values. Only those vertical shifts are allowed which do not cause the crossing point (potential where $\Delta\gamma_\theta = 0$) to be moved outside the limits imposed by the hysteresis loop on the (0,1) intensity plot. The curve for the organic free $KClO_4$ solution has the smallest slope and hence, the vertical displacement of the $\Delta\gamma_\theta$ plots will cause the largest shift of the crossing point potential for this solution. In Fig. 7, dashed vertical lines mark the positive and the negative limits of the hysteresis loop for the $KClO_4$ solution. One can easily see that a vertical displacement of the $\Delta\gamma_\theta$ curves by -2 mN m^{-1} will move the crossing point potential outside the hysteresis loop in the positive direction and a displacement by 4 mN m^{-1} will move this point outside the hysteresis loop in the negative direction. Therefore, the limits become -2 mN m^{-1} $< (\gamma_{Q=0}(R) - \gamma_{Q=0}(U)) < 4$ mN m^{-1}. This provides an estimate for the upper and lower error bar for all values of $\Delta\gamma_\theta$ shown in Fig. 7. The error bars are apparently small in comparison with the magnitude of the driving forces.

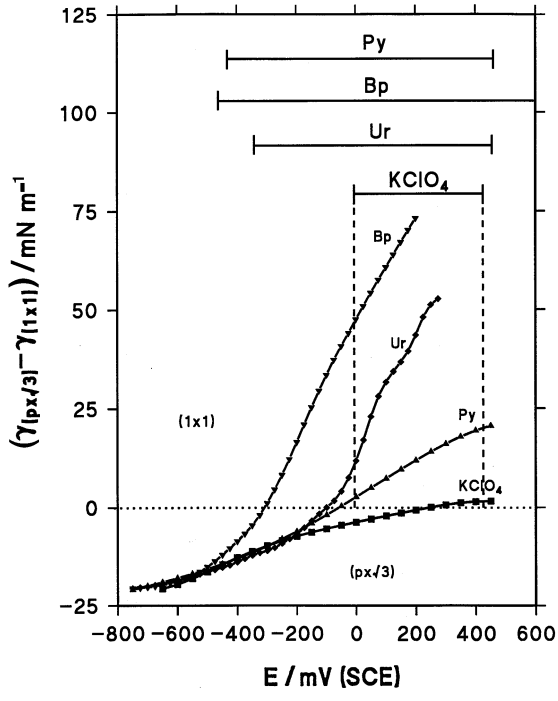

Fig. 7. Difference between the surface energy for the $(p \times \sqrt{3})$ and the (1×1) surfaces, $\Delta\gamma_\theta$, versus the electrode potential in 0.1 M $KClO_4$ in the absence and presence of 1.0×10^{-2} M each of pyridine, 2,2′-bipyridine and uracil. The bars indicate the potential range of the hysteresis loop on the (0,1,0.2) reflection intensity curves shown in Fig. 2.

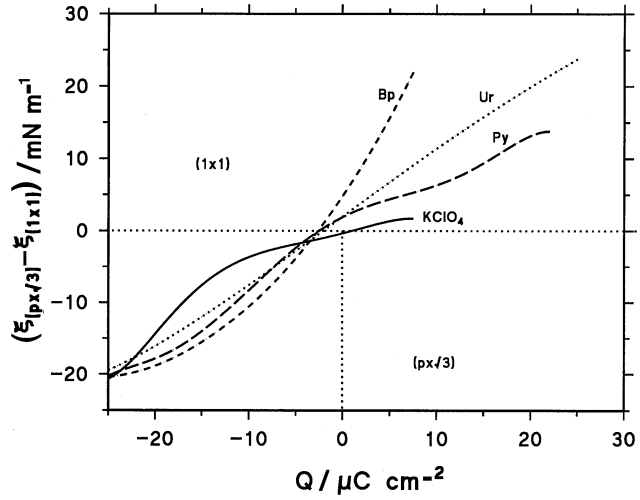

Fig. 8. Difference between the Parsons function for the $(p \times \sqrt{3})$ and the (1×1) surfaces, $\Delta\xi$, versus the charge at the metal for 0.1 M $KClO_4$ in the absence and presence of 1.0×10^{-2} M each of pyridine, 2,2′-bipyridine and uracil.

At this point, we may calculate the driving force for the reconstruction at constant charge. If we assume that $(\gamma_{Q=0}(R) - \gamma_{Q=0}(U)) = 0$, then the driving force becomes equal to:

$$\Delta\xi_\theta = \left(\int_{Q=0}^{Q_E} E_{\theta=0}(R)\mathrm{d}Q - \int_{Q=0}^{Q_E} E_{\theta=0}(U)\mathrm{d}Q \right) - \Delta\phi \tag{13}$$

The right hand side of Eq. (13) can be calculated from the experimental charge density data and the actual driving force for the phase transition may be found within the interval -2 to $+4$ mN m^{-1} around the calculated value. Fig. 8, shows the calculated values of $\Delta\xi$ as a function of the charge. The positive values of $\Delta\xi$ correspond to the region where the (1×1) surface is more stable while the negative values of $\Delta\xi$ correspond to the region where the reconstructed $(p \times \sqrt{3})$ surface is more stable. The point at which $\Delta\xi$ crosses the zero line corresponds to the charge density, Q_T, at which the phase transition should occur. We recall that the driving force in the presence of the organic molecules is given by $\Delta\xi_\theta = \Delta\xi_{\theta=0} - \Delta\phi$ and that the curve for the pure $KClO_4$ shows the values for $\Delta\xi_{\theta=0}$ as a function of Q. Therefore, the solid line in Fig. 8 shows the driving force due to the charge on the metal and the

curves obtained in the presence of the organic molecules show the overall driving force due to the charge and to the adsorbate. These results show beyond any doubt that in the presence of organic adsorbates, the driving force of the transition depends not only on the electric field, but also on the differences in the strength of adsorption of the adsorbate. In the present case, the driving forces due to the adsorbate and to the charge are of a comparable magnitude, at a negatively charged surface. However, at positive charges, the driving force due to adsorption is larger than the force due to the charge. We note that all $\Delta\xi$ curves cross the zero line at a charge of about -3 $\mu C\ cm^{-2}$. This value appears to be consistent with predictions of the electronic theories [21–23]. In reality, the value of Q_T corresponds to the charge at which the $\Delta\phi$ curves for the three organic compounds crossed the zero line in Fig. 6. For the three organic molecules, the driving forces due to charge and due to the adsorbate are synergistic. When the surface is negatively charged, the adsorption is stronger at the reconstructed surface but at positive charge the adsorption is stronger at the unreconstructed surface. The character of adsorption changes near zero charge. However, we do not see a significant change of the charge density Q_T, due to the adsorption of these compound. This behavior may be an exception rather than a rule. The three organic molecules are aromatic heterocyclic compounds. They are all π-bonded to gold at the negatively charged surface and N-bonded to gold at the positively charged surface. The character of their surface coordination changes around the zero charge. Different surface behavior and therefore different contributions to the driving force of the surface reconstruction may be observed for other adsorbates.

The above results indicate that the driving force of the $(p \times \sqrt{3}) \rightarrow (1 \times 1)$ transition is larger and that the kinetics are slower in the presence of organic molecules. These trends seem to be contradictory, since a larger driving force should speed up rather than slow down this surface reaction. This contradiction may be reconciled however, if we take into account that the mechanism of this phase transition involves nucleation and growth of the nuclei of the new phase [29]. The kinetics of the $(p \times \sqrt{3}) \rightarrow (1 \times 1)$ transition are determined by the ability to form critical nuclei of the new phase and the mobility of the gold adatoms. Apparently, the organic molecules hinder the nuclei formation, either by blocking the sites at which these nuclei are formed and/or by slowing down the mobility of gold adatoms. Under these conditions, the surface may remain in the 'supersaturated' state even if the driving force for the phase transition increases.

4. Summary and conclusions

We have investigated the impact of adsorption of three selected organic molecules on the driving force for the $(p \times \sqrt{3}) \rightarrow (1 \times 1)$ phase transition. We have demonstrated that the analysis of the driving forces should be carried out at constant charge. The overall driving force may then be expressed as a sum of the force due to charge and the force of adsorbate. The driving force due to charge is equal to the difference between the surface energy of $(p \times \sqrt{3})$ and (1×1) surfaces measured in absence of the adsorbate (non-adsorbing electrolyte). The driving force due to adsorbate is equal to the negative of the difference between the surface pressure of the adsorbate at the reconstructed and unreconstructed surfaces. The kinetics of the phase transitions are slow in a nonadsorbing electrolyte and in the presence of organic adsorbates. A large hysteresis between the lifting and the formation of the reconstruction is observed in these cases. Due to the slow kinetics of the surface reconstruction, the charge densities for the $(p \times \sqrt{3})$ and (1×1) surface can be measured for potentials where a given structure of the surface exists only as a metastable state [29,33]. We have shown that the driving force for reconstruction due to the adsorbate may be calculated by integration of the charge density data. The calculations of the driving force due to charge were more complex. The charge densities for nonadsorbing electrolyte were used to determine the charge dependence of the difference between the surface energy for the reconstructed and unreconstructed surface. The driving force due to charge was then calculated by making an estimate of the difference between the surface energies at the zero charge on the metal. The potentials of lifting and restoring the reconstruction, taken from the SXS data were used to give the upper and lower limits to this estimate. Our estimate shows that, at zero charge, the difference between the surface energy at the reconstructed and unreconstructed Au(111) surface ranges between -2 to 4 $mN\ m^{-1}$. We have demonstrated that, with the three organic molecules, the driving forces due to charge and due to adsorbate are of a comparable magnitude. This result answers the following statement made in a recent paper devoted to the theory of the surface reconstruction phenomena [23]. At present it is unknown whether the phase transition occurs purely due to the field effects or if the adsorbate is very important. We have shown that the contribution of adsorbates to the surface reconstruction phenomena is important. In the presence of adsorbates, both the adsorbate and the charge contribute to the driving force of the phase transition. Therefore, the interpretation of the surface reconstruction phenomena given in terms of either a purely charge or a purely adsorbate effect has to be considered as an oversimplification. Finally, we would like to emphasize

that our analysis works well when adsorption slows down the surface reconstruction phenomena. In the opposite case, when adsorbates accelerate this phase transition (for example adsorption of halides), the protocol described by Gao et al. [48] may be followed, and the thermodynamic potential of the phase transition may be taken as the potential at which the reconstruction is lifted.

Acknowledgements

The above work was supported by NSERC and by US DOE under contract DE-AC0276CH00016. Th.W. acknowledges the Deutsche Forschungsgemeinschaft (Wa-879/1) for a Heisenberg Award and J.L. thanks the Alexander von Humboldt Stiftung for a Research Award. The authors acknowledge helpful discussions with Dr J. Wang.

References

[1] (a) M.A. Van Hove, S.Y. Tong, (Eds), The Structure of Surfaces I, Spinger, Berlin, 1985; (b) J.F. van der Veen, M.A. Van Hove, (Eds), The Structure of Surfaces II, Springer, Berlin, 1988; (c) S.Y. Tong, M.A. Van Hove, K. Takayanagi, X.D. Xie, (Eds), The Structure of Surfaces, Springer, Berlin, l991.
[2] G.A. Sarnorjai, Introduction to Surface Chemistry and Catalysis, Wiley, New York, 1994.
[3] J. Lipkowski, P.N. Ross (Eds), Structure of Electrified Interfaces, VCH, New York, 1993.
[4] J.V. Barth, H. Brune, G. Ertl, R.J. Behm, Phys. Rev. B 42 (1990) 9307.
[5] D. Gibbs, B.M. Ocko, D.M. Zehner, S.G.J. Mochrie, Phys. Rev. B 42 (1990) 7330.
[6] A.R. Sandy, S.G.J. Mochrie, D.M. Zehner, K.G. Huang, D. Gibbs, Phys. Rev. B 43 (1991) 4667.
[7] (a) D.M. Kolb, in: J. Lipkowski, P.N. Ross (Eds), Structure of Electrified Interfaces, VCH, New York, 1993; (b) D.M. Kolb, Progress in Surface Science, 51 (1996) 109.
[8] B.M. Ocko, J. Wang, A. Davenport, H. Isaacs, Phys. Rev. Lett. 65 (1990) 1466.
[9] B.M. Ocko, G. Helgessen, B. Schardt, J. Wang, Phys. Rev. Lett 69 (1992) 3350.
[10] X. Gao, A. Hamelin, M.J. Weaver, Phys. Rev. B 44 (1991) 10983.
[11] X. Gao, A. Hamelin, M.J. Weaver, Phys. Rev. B 46 (1992) 7096.
[12] X. Gao, G.J. Eden, A. Hamelin, M.J. Weaver, Surf. Sci. 296 (1993) 333.
[13] N.J. Tao, S.M. Lindsay, Surf. Sci. Lett. 274 (1992) L546.
[14] O.M. Magnussen, J. Hotlos, R.J. Behm, N. Batina, D.M. Kolb, Surf. Sci. 296 (1993) 310.
[15] D.M. Kolb, A.S. Dakkouri, N. Batina, in: A.A. Gewirth, H. Sigenthaler, (Eds.), Nanoscale Probes of the Solid/Liquid Interface, NATO ASI Serie C, vol. 288, Kluwer, Dordrecht, 1995, p. 263.
[16] L.M. Tidswell, N.M. Markovic, P.N. Ross, Surf. Sci. 317 (1994) 241.
[17] J. Wang, B.M. Ocko, A.J. Davenport, H.S. Isaacs, Science 255 (1992) 1416.
[18] A. Friedrich, B. Pettinger, D.M. Kolb, G. Lubke, R. Steinhoff, G. Marowsky, Chem. Phys. Lett 63 (1989) 123.
[19] D. Tomanek, K.H. Bennemann, Surf. Sci. 163 (1985) 503.
[20] V. Heine, L.D. Marks, Surf. Sci. 165 (1986) 65.
[21] C.L. Fu, K.M. Ho, Phys. Rev. Lett. 63 (1989) 1617.
[22] A.A. Kornyshev, I. Vilfan, Electrochim. Acta 40 (1995) 109.
[23] K.P. Bohnen, K.M. Ho, Electrochim. Acta 40 (1995) 129.
[24] J. Wang, B.M. Ocko, A.J. Davenport, H.S. Isaacs, Phys. Rev. B 46 (1992) 10321.
[25] B.M. Ocko, O.M. Magnussen, R.R. Adzic, J. Wang, Z. Shi, J. Lipkowski, J. Electroanal. Chem. 376 (1994) 1384.
[26] F. Henglein, D.M. Kolb, J. Lipkowski, Surf. Sci. 291 (1993) 325.
[27] U.W. Hamm, D.M. Kolb, J. Electroanal. Chem. 332 (1992) 339.
[28] Th. Dretschkow, A.S. Dakkuri, Th. Wandlowski, Langmuir 13 (1997) 2843.
[29] Th. Wandlowski, B.M. Ocko, O.M. Magnussen, S. Wu, J. Lipkowski, J. Electroanal. Chem. 409 (1996) 155.
[30] F. Cunha, N.J. Tao, Phys. Rev. Lett. 75 (1995) 2376.
[31] G. Lang, K.E. Heusler, J. Electroanal. Chem. 377 (1994) 1.
[32] R. Parsons, S. Trasaffi, J. Electroanal. Chem. 205 (1986) 359.
[33] Th. Dretschkow, N.J. Tao, Th. Wandlowski, (in preparation).
[34] J. Richer, J. Lipkowski, J. Electrochem. Soc. 133 (1986) 121.
[35] J. Lipkowski, L. Stolberg, in: J. Lipkowski, P.N. Ross (Eds.), Molecular Adsorption at Metal Electrodes, VCH, New York, 1991.
[36] J. Leceour, These de Doctorat, Paris, 1979
[37] A. Hamelin, in: J.O'M. Bockris, B.E. Conway, R.E. White (Eds.), Modern Aspects of Electrochemistry, vol. 16, ch. 1, Butterworth, London, 1979.
[38] D.M. Kolb, J. Schneider, Electrochim. Acta 31 (1986) 929.
[39] J. Leceour, J. Andro, R. Parsons, Surf. Sci. 114 (1982) 320.
[40] P. Skoluda, M. Holzle, J. Lipkowski, D.M. Kolb, J. Electroanal. Chem. 358 (1993) 343.
[41] R. Parsons, Solid State Ionics 94 (1997) 91.
[42] W. Haiss, J.K. Sass, J. Electroanal. Chem. 386 (1995) 267.
[43] W. Haiss, J.K. Sass, J. Electroanal. Chem. 410 (1996) 119.
[44] H. Ibach, C.E. Bach, M. Giessen, A. Grossmann, Surf. Sci. 375 (1997) 107.
[45] J. Lipkowski, W. Schmickler, J. Electroanal. Chem. (in preparation).
[46] R. Parsons, Proc. R. Soc. Lond. Ser. A 261 (1961) 79.
[47] P.N. Ross, A.T. D'Agostino, Electrochim. Acta 37 (1992) 615.
[48] X. Gao, G.J. Edens, M.J. Weaver, J. Elecroanal. Chem. 376 (1994) 21.